processes

MDPI

Article

Fabrication and Characterization of Hydrophobic Porous Metallic Membranes for High Temperature Applications

Sara Claramunt *, Muhammad Khurram, Walther Benzinger, Manfred Kraut and Roland Dittmeyer

Institute for Micro Process Engineering (IMVT), Karlsruhe Institute of Technology, 76131 Karlsruhe, Germany; muhammadkhurram56@gmail.com (M.K.); walther.benzinger@kit.edu (W.B.); manfred.kraut@kit.edu (M.K.); roland.dittmeyer@kit.edu (R.D.)

* Correspondence: sara.claramunt@kit.edu; Tel.: +49-721-608-24052

Abstract: Hydrophobic porous metallic membranes can be integrated in a microreactor for in situ separation of steam at high temperatures. This study investigates the fabrication and characterization of hydrophobic coatings on metallic substrates. Two different coating methods were explored: (1) Plasma Enhanced—Chemical Vapor Deposition (PE-CVD) to form amorphous carbon silicon-doped a-C:H:Si:O thin films and (2) Direct Immersion in fluoroalkyl silane (FAS-13) solution using dip coating to form Self-Assembled Monolayers. The results on wettability as well as SEM images and EDS/WDS analyses indicate that the coated sintered stainless steel membranes are adequate as hydrophobic surfaces, maintaining the porosity of the substrate and withstanding high temperatures. Especially the FAS-13 coating shows very good resistance to temperatures higher than 250 °C. These findings are of special significance for the fabrication of porous metal membranes for separation of steam in high temperature applications.

Keywords: porous metal membrane; hydrophobic; plasma enhanced—chemical vapor deposition; amorphous carbon layer; dip coating; FAS; high temperatures; stainless steel

Citation: Claramunt, S.; Khurram, M.; Benzinger, W.; Kraut, M.; Dittmeyer, R. Fabrication and Characterization of Hydrophobic Porous Metallic Membranes for High Temperature Applications. *Processes* **2021**, *9*, 809. https://doi.org/10.3390/pr9050809

Academic Editor: Moisès Graells

Received: 31 March 2021
Accepted: 30 April 2021
Published: 5 May 2021

1. Introduction

Process intensification in microstructured devices can be pursued by combining in situ two unit operations: chemical reaction and separation. For instance, the equilibrium of certain polycondensation reactions, for example, producing branched polysaccharides, can be displaced towards a higher yield when the by-product (in this case, water) is removed through a membrane. The membrane should be hydrophobic to block the passage of the target product (aqueous reactive solution) while allowing water in vapor state to enter the pores. This specific polycondensation reaction, when performed in a microreactor with short and well defined residence time, needs rather high temperatures (230–250 °C) for obtaining high yield and selectivity. Such high temperatures imply several challenges for the membrane, like the adequacy of the material for the reaction conditions and suitable surface properties to prevent the reaction product from entering the pores [1].

Stainless steel (SS) porous membranes exhibit high thermal resistance but also a high surface energy (that is, hydrophilic behavior), which facilitates the wetting of the pores. Hydrophobic membranes are commonly prepared by increasing the surface roughness and/or by chemical modification [1,2]. Surface roughness may either lead to the so-called Wenzel or Cassie–Baxter wettability state (see Figure 1), which reflects a modification of the contact angle in comparison to a perfectly flat surface [3]. In the Wenzel state [4], the wetting liquid penetrates the roughness grooves or pores. For pore geometries where gas is trapped, that is, the Cassie–Baxter state [5], the contact area between the liquid and the solid surface is reduced, thus leading to an enhancement of the contact angle. An intermediate state, where the liquid partially wets the surface is also commonly encountered [6].

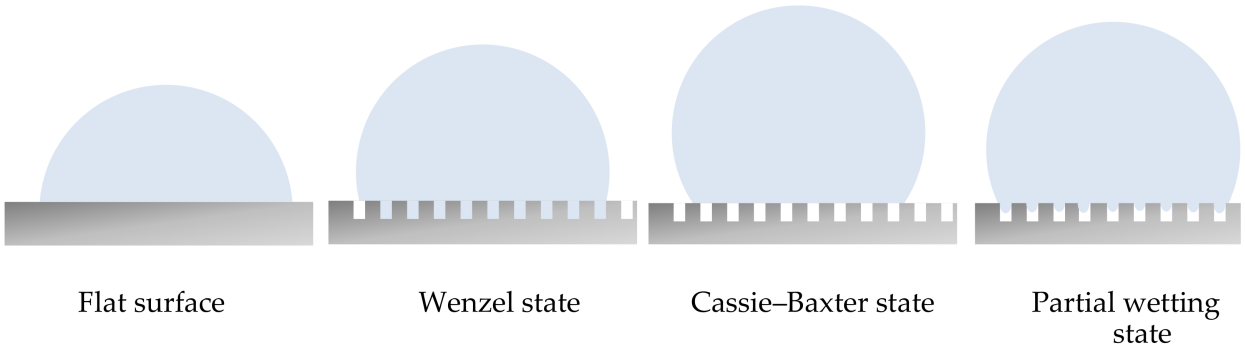

Figure 1. Wettability states in flat and rough (porous) substrates.

The chemical modification of metallic surfaces to render them hydrophobic has been investigated using different methods like the sol-gel method [7,8], direct immersion in a reactive hydrophobic solution [9], electrodeposition [10], thermal plasma evaporation [11], and Plasma Enhanced—Chemical Vapor Deposition (PE-CVD) [12].

Organosilicon compounds can be grafted into hydrophilic surfaces employing PE-CVD to form hydrophobic thin films on various substrates [13]. Amorphous carbon layers (a-C:H) are also known as Diamond-like-carbon (DLC) layers due to the high amount of sp^3 hybridized C atoms which gives them diamond-like properties [14]. These layers can be doped using Si and O (a-C:H:Si:O) to produce highly hydrophobic coatings [15–20] by incorporating organosiloxane compounds like hexamethyldisiloxane (HMDSO) as a liquid precursor in the PE-CVD process [12,13]. Only a small amount of solvent is needed, and heat is required to vaporize the organosiloxane compound [21].

In contrast to CVD grafting, immersion grafting is a wet method. The membrane is immersed directly into a reactive organosilane liquid solution [1], for example, a fluoroalkyl silane (FAS). This reactive solution is previously prepared by hydrolyzing the organosilane compound in solvents such as water or alcohol [22]. When the substrate is immersed in the FAS solution, the FAS molecules are chemisorbed on the hydrophobic surfaces [1]. This coating method often results in highly organized needle structures, also known as Self-Assembled Monolayers (SAM) [23].

The applicability of hydrophobic coatings on porous substrates such as hydrophobic membranes can be evaluated by the characterization of the Liquid Entry Pressure. The Liquid Entry Pressure (LEP) is defined as the minimum pressure that can be applied before a liquid penetrates the pores of a dry membrane [19]. It depends on the surface tension of the wetting liquid, the contact angle, and the pore size and geometry of the membrane itself. For a given porous substrate with a given pore size distribution, the higher the hydrophobicity of the surface is, the higher the Liquid Entry Pressure will be. Thus, if the LEP is not exceeded, the membrane shows resistance to pore flooding and steam separation can still take place. As soon as the LEP is exceeded, pores get increasingly flooded, the water vapor transport rate gets reduced, and a liquid flow arises [24].

The application of hydrophobic membranes fabricated by the two above mentioned coating techniques were focused on ambient or moderate temperatures [12,25]. With a view to the application envisaged, there is a need to characterize these hydrophobic coatings for their performance in separation tasks at elevated temperatures. Thus, in the present work (see Figure 2) we report the fabrication of high-temperature-resistant hydrophobic coatings on porous metal substrates by: (1) Plasma-Enhanced Chemical Vapor Deposition of silicon doped DLC thin films (a-C:H:Si:O, also known as Si-DLC); and, alternatively, by: (2) Direct immersion in a Fluoroalkylsilane compound (FAS) to form Self-Assembled Monolayers (SAMs).

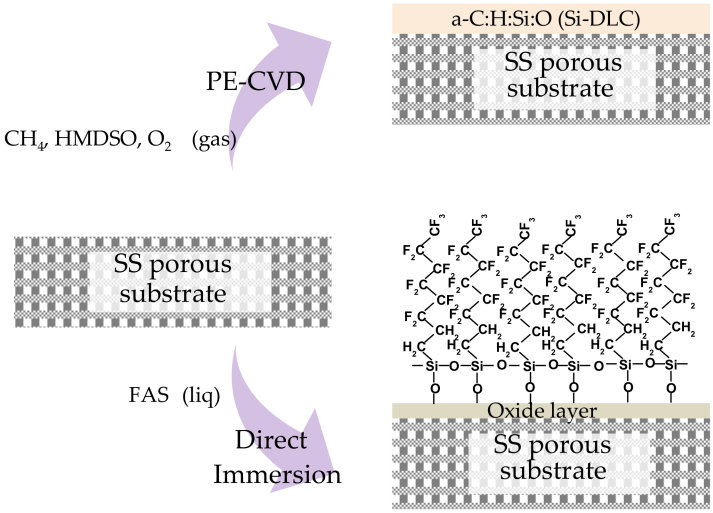

Figure 2. Schematic overview of the processes applied in this study.

The hydrophobic coatings were characterized qualitatively and quantitatively with respect to hydrophobicity, homogeneity, resistance to elevated temperatures, and Liquid Entry Pressure.

2. Materials and Methods

2.1. Materials

To better characterize the coating itself and to avoid the influence of the substrate surface characteristics on the coatings, the coating was first investigated on flat surfaces, that is, silicon wafers <100> (Siegert Wafer GmbH) and flat stainless steel (SS) flat plates, see Figure 3a. Figure 3b–d shows a SEM image of the cross-section of the stainless steel substrates. The total thickness of the substrates is given in Table 1.

Table 1. Metallic substrates used in this study.

Substrate Material	Structure	Total Thickness
Silicon (wafer)	flat	0.5 mm
Stainless steel	flat	0.3 mm
Stainless steel	porous (52%) [1]	2 mm
Stainless steel	porous (40%) [2]	2 mm
Stainless steel	Fine porous [3]	3 mm

[1] Sika R-100 (52% porosity), [2] Sika R-15 (40% porosity), [3] Sika R-AS.

The coatings were investigated further on porous sintered stainless steel substrates (GKN Sinter Metals Filters GmbH) with different porosities. The fine porous substrate (Figure 3d) is an asymmetric porous metal membrane and is the result of two consecutive sintering processes with different metal powder particle sizes. This results in a 140–170 µm thick top layer of sintered fine metal powder. For investigation of the coating characteristics, a standard size of 10 × 20 mm for all substrates was used.

The gases employed in the PE-CVD coating process were argon (99.9999%, Alpha Gaz by Air Liquide), hydrogen (99.9999%, Alpha Gaz by Air Liquide), oxygen (99.998%, Alpha Gaz by Air Liquide), nitrogen (99.9999%, Alpha Gaz by Air Liquide) and methane (4.5 purity > 99.995%, Basi Schöberl). HMDSO (Assay GC area% > 98.5, Merck KGaA) is obtained as a liquid but is used in a gaseous state in the system.

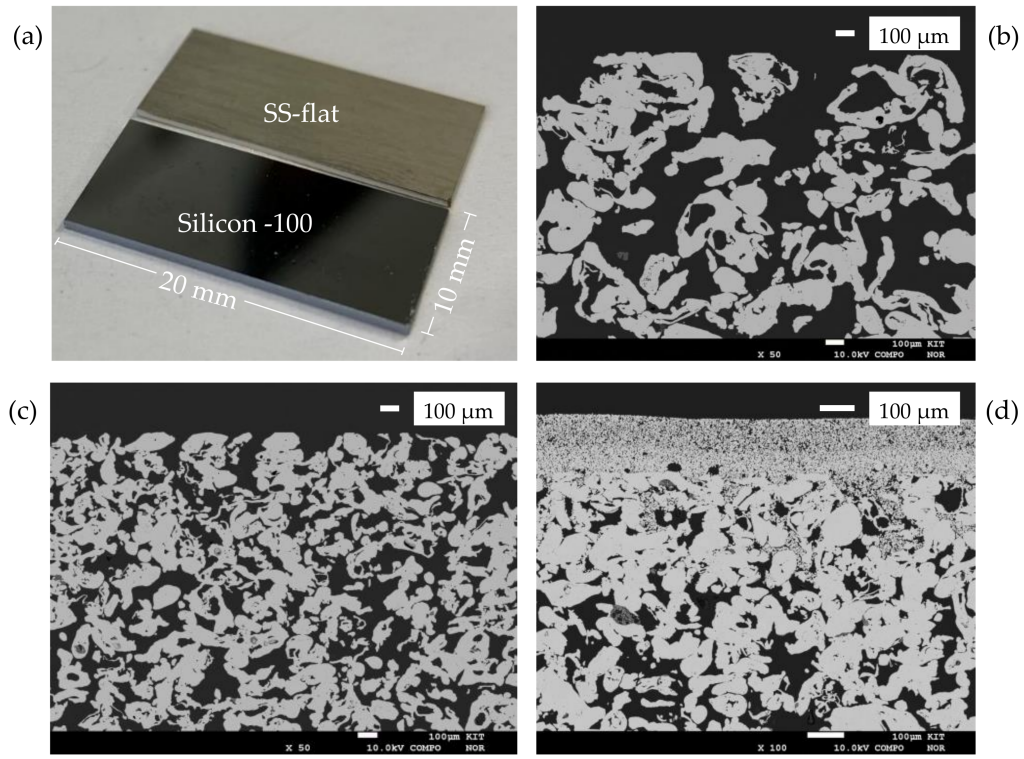

Figure 3. Overview of the used substrates: (**a**) silicon and stainless steel (SS) flat substrates; (**b**) 52% porous SS substrate; (**c**) 40% porous SS substrate; and (**d**) fine porous multilayer SS substrate.

The chemicals used for direct immersion in FAS were 1H,1H,2H,2H-Perfluorooctyltriethoxysilane (FAS-13) (98%, Sigma Aldrich), Ethanol (99.9%, Merck KGaA), HCl (32%, Merck KGaA), and deionized water.

In addition, acetone (99.7%, Carl Roth GmbH), isopropanol (99.5% Carl Roth GmbH), and deionized water were used for pre-processing (cleaning) of the substrates.

2.2. Coating Methods

Two different coating methods were applied for grafting to modify the chemistry of the metallic surfaces and render them hydrophobic:

- *Plasma-Enhanced Chemical Vapor Deposition (PE-CVD) of thin films.* Amorphous diamond-like carbon (DLC) thin film layers doped with silicon and oxygen (a-C:H:Si:O) were deposited using a combined PVD/PECVD System (STARON 60-60, PT&B Silcor) at 180 °C and 1.5 Pa chamber pressure operated with a radiofrequency power of the plasma source of 100 W. To fabricate the a-C:H:Si:O coating [12], HMDSO (4 Ncm^3/min), argon (40 Ncm^3/min), and methane (150 Ncm^3/min) were used as precursors. To obtain a homogeneous coating thickness [12], the samples were rotated during coating with 4 rpm rotating speed. The coating duration was 1 h.
- *Direct immersion in FAS solution.* The direct immersion of the substrates was performed by dip coating (dip coater with motorized actuator—AZ Series, Software MEXE02) in FAS-13 solution. The solution was prepared in ethanol (absolute) with 1.66 wt.% FAS-13 and 1.66 wt.% HCl (32%)—hydrolyzed by the addition of a threefold molar excess of water at room temperature. The solution was stirred for 5 h and held for 24 h at ambient temperature before being used for coating. The substrates were completely immersed in the FAS solution using the dip coater technique with 3 mm/min withdrawal speed and 30 s coating immersion time at room temperature. The grafted membranes were then dried for 2 h at 70 °C in a drying chamber (Series KMF, Binder GmbH). Afterwards, the samples were transferred to a muffle furnace

(Heraeus Thermo Scientific, Waltham, MA USA), heated from room temperature up to 200 °C with a heating rate of 0.5 °C/min, and kept at 200 °C for 6 h.

- *Pre-processing*: The metal substrates were cleaned in an ultrasonic bath (Elba X-tra 70H) in the presence of acetone, isopropanol, and water successively for 30 min respectively [9] and finally dried in a drying chamber (Series KMF, Binder GmbH) at 70 °C during 5 min. In the case of the FAS modification of the SS samples, they were immersed in a pickling solution consisting of 1:1 in volume dilution of the commercial HCl in water for 5 min at room temperature, washed with deionized water, and blown dry [9].

2.3. Characterization

2.3.1. Coating Characteristics

The coatings were characterized by optical profilometry (SensoFar S neox, Sensofar-Tech). The coatings were also investigated using Scanning Electron Microscopy (SEM) and Electron Probe Microanalysis (EPMA) with a Field Emission Electron Probe Microanalyzer (JXA-8530F, JEOL Ltd.). For cross-sectional SEM characterization, samples were embedded in epoxy resin, ground, polished, and finally sputtered with a conductive layer of platinum to avoid charging. The presence of certain elements in the layer was determined qualitatively by Energy-dispersive spectroscopy (EDS) and Wavelength-dispersive spectroscopy (WDS).

2.3.2. Contact Angle

The contact angle (CA) formed by sessile drops of deionized water was measured at ambient conditions with a contact angle goniometer (OCA 5, Data physics) before and after the coating according to the standards [26], to evaluate the impact of the coating's hydrophobicity.

2.3.3. Thermal Stability

The heating of the coated samples for endurance tests at high temperature was performed in the muffle furnace (Heraeus Thermo Scientific, Waltham, MA USA) for different holding times and a common heating rate of 2 °C/min.

2.3.4. Liquid Entry Pressure

To characterize the applicability of the coated membranes as hydrophobic membranes, Liquid Entry Pressure (LEP) tests were performed. Visual detection was used to determine at which pressure the first drop arose in the membrane backside. For the tests, a setup according to [12] was used. Here, a manual screw pump was used to step-wise pump deionized water in the Poly(methyl methacrylate) test cell where the 20 × 10 mm-coated substrate was clamped in dead end mode. The pressure was increased 0.1 bar each time and held for 30 s. The pressure at which a water droplet was visible through a USB digital microscope on the backside of the membrane was recorded using a pressure transmitter.

3. Results and Discussion

3.1. Coating Characteristics

The coating thickness, morphology, and quality of the surface were analyzed by Scanning Electron Microscopy and profilometry. The right side of each sample was covered with Kapton® tape before coating to compare the surface of the coated and uncoated material after completion of the surface modification process:

- Silicon Doped DLC (PE-CVD)

Figure 4 shows the top view of the Si-DLC coatings on a silicon wafer (a), the SS plate (b), and the SS porous substrate (c,d). A homogeneous coating can be observed. Profilometry of the coatings reveals an average thickness of 440 nm for a 1-h coating. The PE-CVD Si-DLC coated surfaces show thin homogeneous films without defects or cracks.

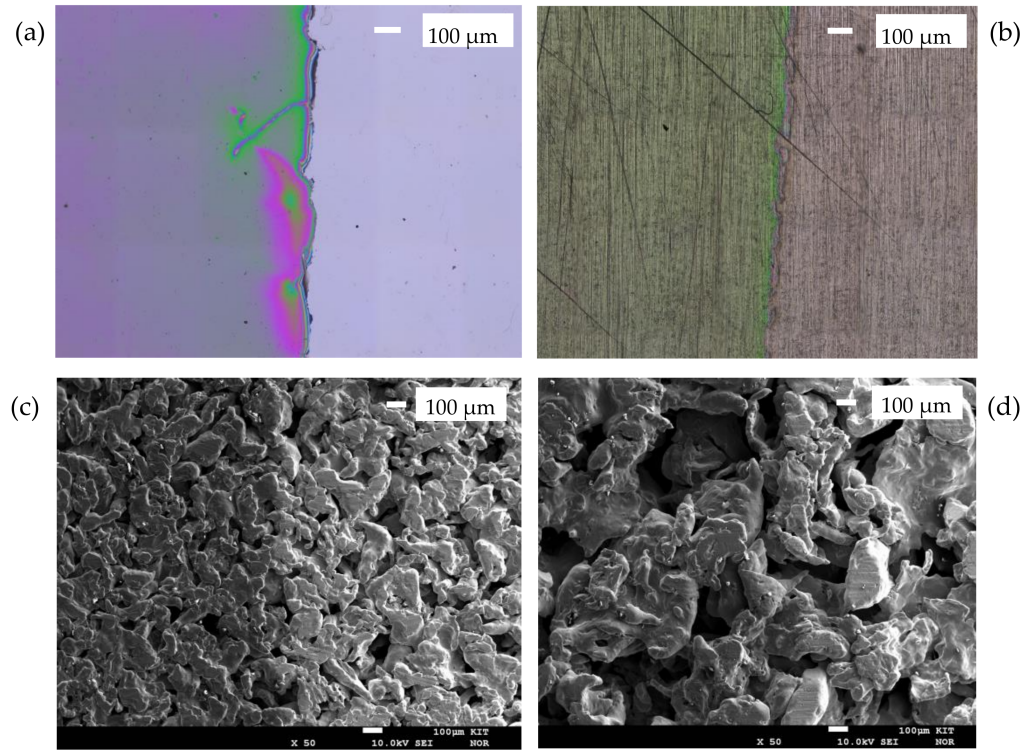

Figure 4. Top view of the coatings on different substrates (left hand side: coated; right hand side: uncoated. (**a**) Si-DLC on silicon substrate—optical profilometry 10×; (**b**) Si-DLC on SS-flat substrate—optical profilometry 10×; (**c**) Si-DLC on SS-40% porous substrate-SEM; (**d**) Si-DLC on SS-52% porous substrate-SEM.

For a better visual representation, Figure 5 shows the cross-section of the Si-DLC coatings on (a) a silicon wafer and (b) a fine porous SS substrate; both for a coating process of 3 h, with an average thickness of 1.4 µm. It can be seen that the inner side of the pores close to the external surface of the sample get coated and that the pores get narrower, which both should prevent the entrance of water into the pores. Figure 5 also reveals that the coating does not block the pores (see white arrows), which shall allow the permeation of steam.

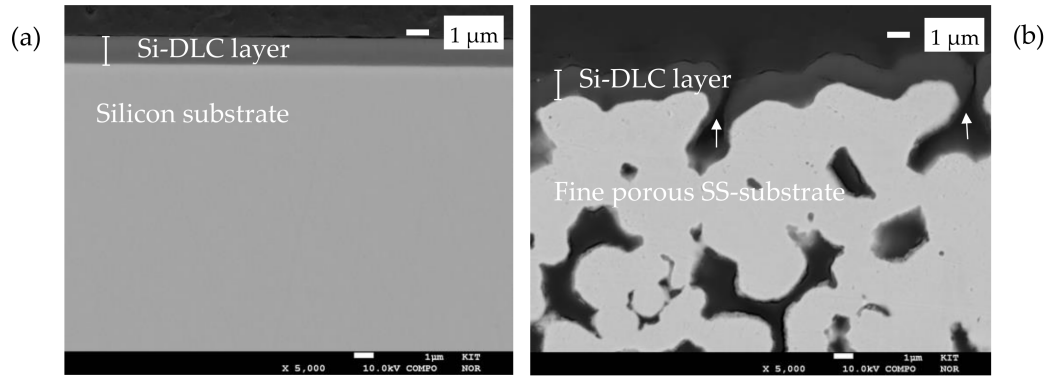

Figure 5. SEM Image of the cross-section of the Si-DLC coating on (**a**) a flat silicon substrate and (**b**) a fine porous SS substrate.

The presence of C, O, and Si according to the EDS results (Table S1 and Figure S1) confirms the development of a homogeneous layer on the metallic substrates.

- FAS Self-Assembled Monolayer (Dip Coating)

Figure 6 shows the top view of the FAS coating on a silicon wafer (a) and a SS flat plate (b,c). In Figure 6a, it can be observed that the FAS coating is transparent. All SS substrates were pickled with HCl before the immersion in the FAS solution, which enhanced the final contact angle. HCl pickling [27]—removal of most external layers (surface contamination and iron layer)—has a great effect on the fabrication of hydrophobic coatings, by increasing the polar component of the surface energy and nano roughness [8]. This effect can be seen in the cavities between the grains in Figure 6b, and with greater detail in Figure 6c. As already mentioned, the coating was transparent. However, it can be seen in Figure 6b that the coated part of the substrate has a darker color, as the emission of secondary electrons differs where the coating layer is present.

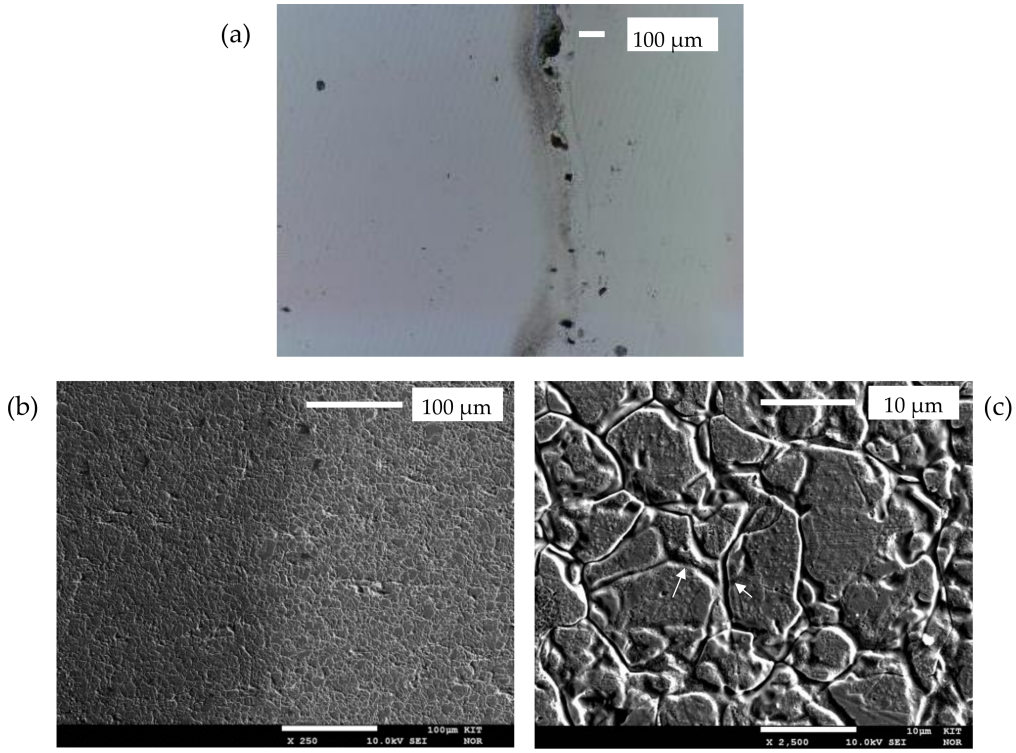

Figure 6. Top view of the coatings on different substrates (left-hand side: coated; right-hand side: uncoated. (**a**) FAS on silicon substrate—optical profilometry 10×; (**b**) FAS on SS-flat substrate—SEM; (**c**) detail of the coated part on the SS-flat substrate: Effect of pickling pre-processing can be seen in the grain boundaries (white arrows).

No profilometric measurements were possible due to the coating transparency as well as the low thickness. The cross-sectional images performed by SEM did not show any layer. However, EDS and WDS analysis of the top side (Table S2 and Figures S1 and S2) confirmed the presence of C, F, and Si all over the surface, which indicated the development of the hydrophobic layer on the metallic substrate.

Figure 7 shows a SEM picture of the coating on a silicon substrate, which reveals a spot-wise agglomeration. EDS analyses revealed a higher concentration of the coating elements in the spots. No cracks were visible on the surface. The agglomeration (dots in Figure 7) might be a consequence of the polycondensation reaction among the reactive organosilane molecules, which leads to the formation of uneven thickness [1].

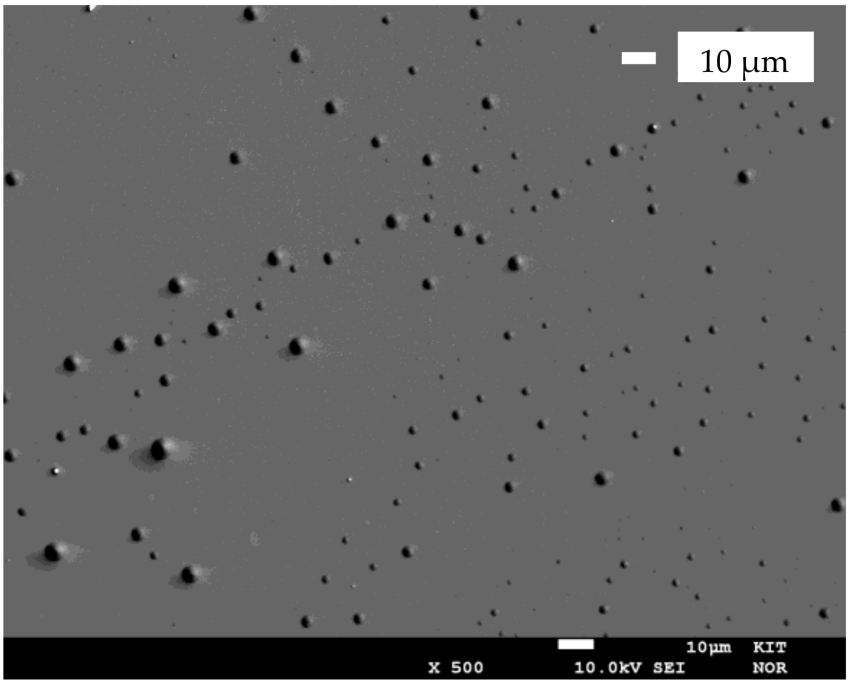

Figure 7. SEM Image of the top view of the FAS coating on a silicon substrate.

In both cases, Si-DLC and FAS coatings, high adhesion, and mechanical robustness could be observed.

3.2. Contact Angle

The hydrophobic behavior of the resulting surface on the different substrates was characterized using contact angle measurements with deionized water. The results obtained are reported in Figure 8. The right and left contact angles of at least three droplets were measured for each substrate sample. The contact angle results shown in Figure 8 represent the average contact angle of at least 10 samples.

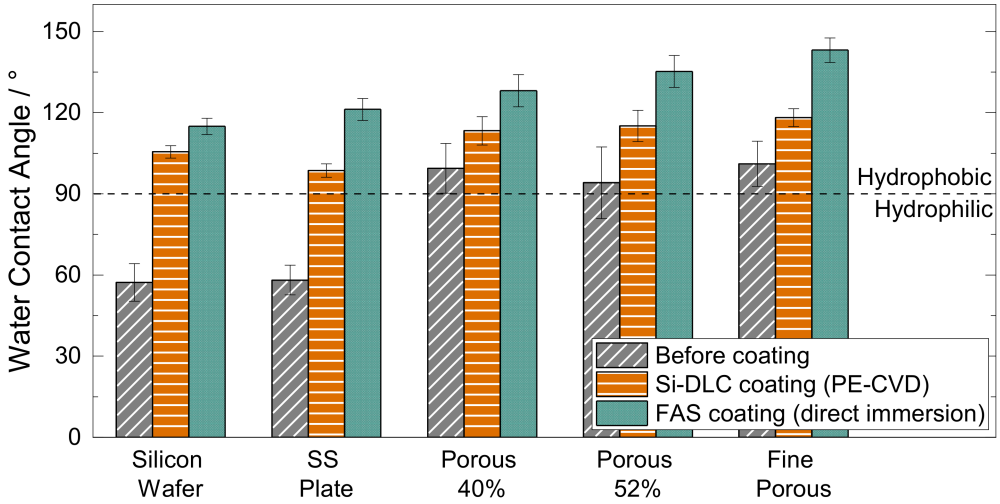

Figure 8. The average contact angle for the different substrates: before coating (grey), after Si-DLC coating (orange) and after FAS coating (green).

The low contact angle of the uncoated substrates is a consequence of the highly hydrophilic nature of the metallic surface, as a result of the high density of the –OH groups

(natural oxide layer) on the surface. Silicon wafers display a surface with the highest surface energy, and therefore lowest contact angle (57° ± 7°) due to not only the presence of a natural oxide layer but also the polished finish of the surface. The contact angle measured before the coating process increases from the flat substrates to the porous substrates as the surface roughness of the materials also does (Table S3 and Figures S9–S12), which may follow the Cassie–Baxter state [5] behavior. However, further AFM studies of the surface roughness would be needed to underpin this interpretation. The highest contact angles were measured for the fine porous substrates (101° ± 8°).

The a-C:H:Si:O coatings turned all the surfaces hydrophobic. The resulting contact angle on the silicon substrate, (105° ± 2) is in agreement with literature data [12,15,19]. In the case of stainless steel flat substrates, somewhat lower contact angles were achieved (99° ± 2°). However, higher contact angle values were obtained, as expected, for the porous stainless steel substrates. In the case of the fine porous substrates, a value of 118° ± 3° was detected.

In the case of the direct immersion in the FAS solution by dip-coating, even higher contact angles were achieved. This is mainly due to the presence of the CF_3 topmost group in the chain when the fluoroalkyl chains are well assembled and vertically aligned [23]. The CF_3 group displays a high hydrophobicity of 120° [28]. When the fluoroalkyl chains are collapsed, the formation of disordered monolayers takes place and the CF_2 is mainly exposed [23]. In the case of the fine porous substrate, almost superhydrophobic surfaces (CA 143° ± 5°) were achieved. The direct immersion in the FAS solution appears to be a very straightforward coating technique leading to improved contact angles in comparison to the Si-DLC coatings. An insight of the hydrophobic behavior of water droplets on the FAS coated fine porous stainless substrates can be taken from Figure 9.

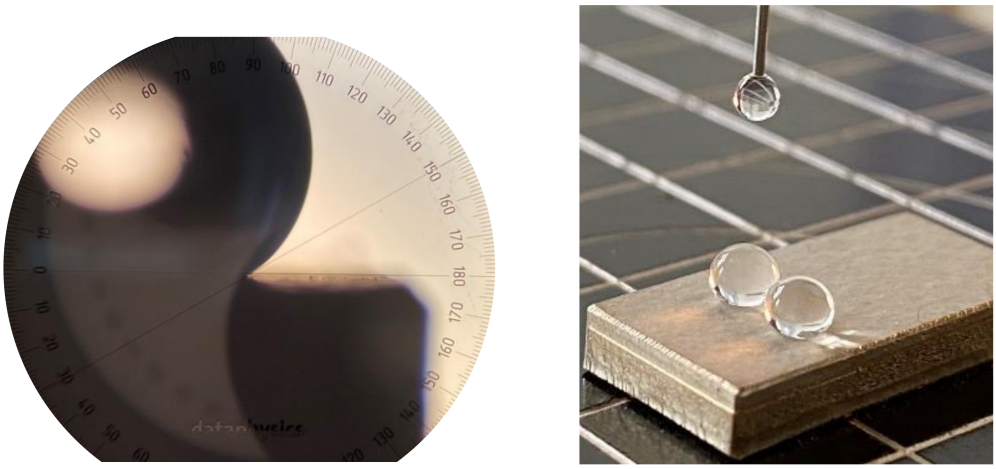

Figure 9. Hydrophobic behavior of water droplets on FAS coated fine porous stainless steel substrates.

3.3. Thermal Stability

To characterize the effects of temperature on the hydrophobic coating surface, coated samples were heated and held to different target temperatures for 2 h with a heating rate of 2 °C/min. After cooling down to room temperature, the contact angle was measured. The same sample was again heated and held at the next target temperature and cooled down for contact angle characterization. Figure 10 shows the water contact angle values after each heating test for the two different coatings on silicon substrates. It can be seen how temperature leads to a degradation of the Si-DLC coating on the surface of the samples. After heating at temperatures higher than 220° C, the hydrophobic behavior has disappeared, showing a contact angle of 87° ± 1°. In the case of the FAS coated silicon wafer substrates, samples remained hydrophobic after a heating to 350 °C. However, a certain degradation can be observed above 300 °C.

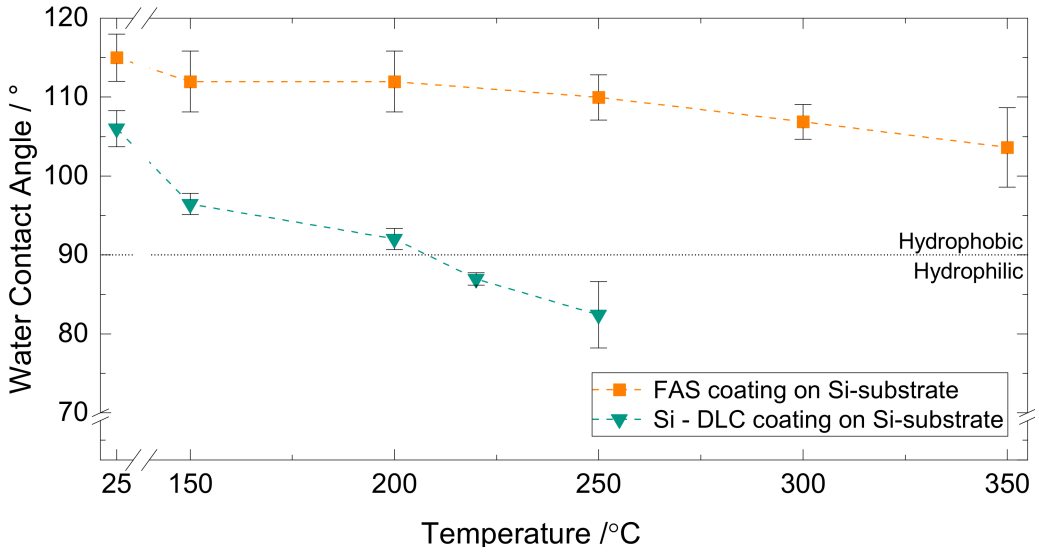

Figure 10. Comparison of the thermal resistance of the different coatings on a silicon substrate.

Figure 11 shows the results of the same test for different substrates coated with the FAS layer. It can be seen how the coatings on the SS samples lose their hydrophobicity already at lower temperatures compared to the coatings on the silicon substrates, that is, at temperatures higher than 275 °C. WDS analyses (Figures S3–S6) show the presence of F in the coating after the last heating to 280 °C. Especially, the coated flat SS substrates developed a blue heat tint on the surface, which is an indication of the growth of the intermediate oxide layer [29–31] leading to an increase of the surface energy and therefore, reduction of the contact angle. The contact angle on coated porous SS substrates decreased with temperature, but did not reach hydrophilic values. In the case of the porous samples, a growth of the oxide layer is also expected. However, the structured surface still maintains a hydrophobic contact angle.

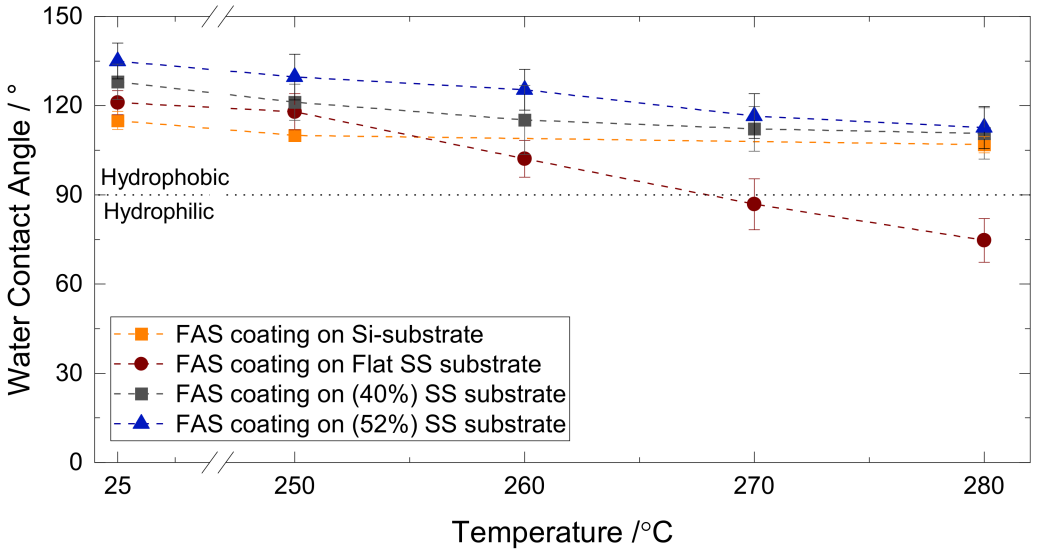

Figure 11. Results of the thermal resistance test for the FAS coating on different substrates.

To probe the adequacy of the coatings for their actual application, the coatings were tested at the target temperature of 250 °C for 2 h. After each heating cycle, the contact angle measurement was repeated to determine after how many cycles at constant temperature the samples lose their hydrophobicity. As per Figure 12, it can be seen that the hydrophobic

behavior of FAS coatings on silicon and porous SS substrates withstood at least 4 heating cycles. WDS analyses on SS coated substrates (Figures S7 and S8) revealed that F is still present in the layer. The decrease in contact angle may be again a consequence of the growth of an oxide layer. In this case, the coating on the flat SS substrate degraded faster than on the porous SS substrates.

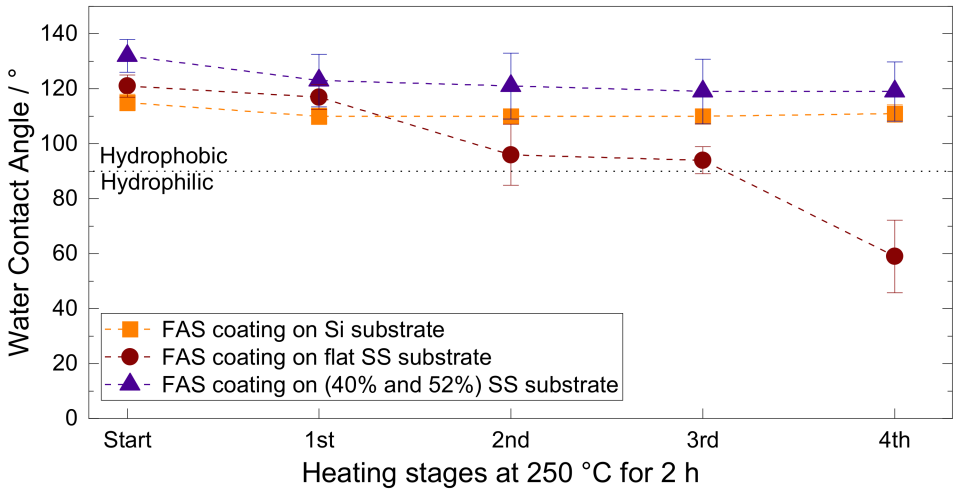

Figure 12. Results of the thermal resistance test for the FAS coating on different substrates.

3.4. Liquid Entry Pressure

The FAS coatings showed higher contact angles and thermal resistance to elevated temperatures in comparison to the Si-DLC coatings. Therefore, FAS coated porous substrates were further characterized according to their Liquid Entry Pressure (LEP). The average results are shown in Table 2.

Table 2. Measured LEP value on the FAS coated SS porous substrates.

Substrate Material	LEP (bar g)
SS porous (52%)	0
SS porous (40%)	0
SS Fine porous	1.3 ± 0.05

The LEP is inversely proportional to the membrane pore size. Therefore, even if hydrophobized and showing high contact angles in the order of 130°, the large pores in the porous (52%) and (40%) SS substrates enable a water breakthrough through the pores at very low-pressure levels (almost no differential pressure). Porous substrates sintered from finer particles reduce the pore size, resulting in an enhancement of the LEP. This value of 1.3 bar (g) indicates a certain flexibility for separation tests to be conducted. However, the influence of higher temperatures on the LEP should also be taken into account. Not only the effect of temperature on structural changes of the coating but also on the surface tension of the wetting fluid should be considered. Higher temperatures involve the reduction of the surface tension [32], causing therefore a further reduction of the LEP [33]. The membrane reactor must be operated in a process window where the LEP of the membrane is not exceeded.

4. Conclusions

When high-temperature conditions are required for a reaction to take place in a membrane reactor, membrane materials are needed which tolerate these temperatures. Metallic membranes are often more robust than ceramic membranes and can be joined easier with other parts of the reactor, which brings advantages for the membrane reactor development, in case, for instance, the pieces are welded in the reactor. The surface of

metallic flat and porous substrates could be hydrophobized using PE-CVD of a Si-DLC layer and alternatively by direct immersion in a FAS solution. The pore inner surface could be coated and blocking of the pores could be avoided, as the SEM images revealed. The FAS coated samples displayed a higher contact angle and a higher thermal resistance than the Si-DLC coated samples. In this work, it has been shown for the first time that these FAS coatings sustain temperatures up to 250 °C without loss of hydrophobic properties. The Liquid Entry Pressure experimental results at ambient conditions indicated that FAS coated fine porous stainless steel substrates have a chance to be applied as membranes for steam separation. Further studies should characterize the coated membranes in terms of Liquid Entry Pressure and permeability at the required operating conditions to prove their suitability for continuous removal of steam at elevated temperatures.

Supplementary Materials: The following materials are available online at https://www.mdpi.com/article/10.3390/pr9050809/s1, Table S1: Average EDS Results for the Si-DLC layer on a porous SS substrate. Probe positions see Figure S1, Table S2: Exemplary EDS results for a FAS coated silicon wafer (including substrate). Probe positions see Figure S1, Figure S1: Probe positions marked for EDS analysis of (a) Si-DLC layer on a porous SS substrate; (b) FAS coated silicon wafer (including substrate), Figure S2. WDS analysis of (a) uncoated silicon wafer, showing the absence of O and F (no peaks); (b) FAS coated silicon wafer, showing the presence of Si, O, and F in the layer, corresponding to Figure S1, Figure S3. WDS Analysis of the FAS coated silicon wafer after 350 °C heating stage, corresponding to the sample in Figure S4, Figure S4. SEM picture of the FAS coated silicon wafer after the 350 °C heating stage, Figure S5. WDS Analysis of the FAS coated flat SS substrate after the 280 °C heating stage corresponding to the sample of Figure S6, still showing the presence of the layer elements, Figure S6. SEM picture of the FAS coated flat SS substrate after the 280 °C heating stage, Figure S7. WDS Analysis of the FAS coated flat SS substrate after 4 heating cycles at 250 °C corresponding to the sample of Figure S8, showing the presence of the layer elements, Figure S8. SEM picture of the FAS coated flat SS substrate after 4 heating cycles at 250 °C, Table S3. Average 3D surface texture parameters according to ISO 25178 [34], performed with confocal microscopy, Figure S9. Exemplary surface height profile of the flat SS substrate (non-coated), Figure S10. Confocal image of a flat SS substrate (non-coated) corresponding to the height profile in Figure S9, Figure S11. Exemplary surface height profile of the fine porous SS substrate (non-coated), Figure S12. Confocal image of a fine porous SS substrate (non-coated), corresponding to the height profile in Figure S11.

Author Contributions: Conceptualization, S.C.; methodology, S.C.; validation, S.C. and M.K. (Manfred Kraut); formal analysis, S.C. and M.K. (Muhammad Khurram); investigation, S.C., M.K. (Muhammad Khurram) and W.B.; resources, S.C., M.K. (Manfred Kraut) and R.D.; data curation, S.C.; writing—original draft preparation, S.C.; writing—review and editing, W.B., M.K. (Manfred Kraut) and R.D.; visualization, S.C. and M.K. (Muhammad Khurram); supervision, M.K. (Manfred Kraut) and R.D.; project administration, M.K. (Manfred Kraut) and R.D.; funding acquisition, M.K. (Manfred Kraut) and R.D. All authors have read and agreed to the published version of the manuscript.

Funding: This research received no external funding.

Institutional Review Board Statement: Not applicable.

Informed Consent Statement: Not applicable.

Data Availability Statement: Not applicable.

Acknowledgments: The authors would like to thank Fabian Grinschek for technical support with the PE-CVD plant; Alexander Navarrete and Kay Marcel Dyrda for providing an apparatus for dip-coating; Leandro Gliosca for performing the first trials; Uta Gerhards and Florian Messerschmidt for SEM and EDS/WDS studies; Torsten Wunsch and Dennis Scherhaufer for substrate preparation and Thomas Gietzelt for fruitful discussions.

Conflicts of Interest: The authors declare no conflict of interest.

References

1. Ahmad, N.A.; Leo, C.P.; Ahmad, A.L.; Ramli, W.K.W. Membranes with Great Hydrophobicity: A Review on Preparation and Characterization. *Sep. Purif. Rev.* **2015**, *44*, 109–134. [CrossRef]
2. Kim, T.-Y.; Ingmar, B.; Bewilogua, K.; Oh, K.H.; Lee, K.-R. Wetting behaviours of a-C:H:Si:O film coated nano-scale dual rough surface. *Chem. Phys. Lett.* **2007**, *436*, 199–203. [CrossRef]
3. Sheng, Y.-J. Effects of geometrical characteristics of surface roughness on droplet wetting. *J. Chem. Phys.* **2007**, *127*, 234704. [CrossRef] [PubMed]
4. Wenzel, R.N. Surface Roughness and Contact Angle. *J. Phys. Chem.* **1949**, *53*, 1466–1467. [CrossRef]
5. Cassie, A.B.D.; Baxter, S. Wettability of porous surfaces. *Trans. Faraday Soc.* **1944**, *40*, 546–551. [CrossRef]
6. Nagayama, G.; Zhang, D. Intermediate wetting state at nano/microstructured surfaces. *Soft Matter* **2020**, *16*, 3514. [CrossRef] [PubMed]
7. Vidal, K.; Gómez, E.; Goitandia, A.M.; Angulo-Ibáñez, A.; Aranzabe, E. The Synthesis of a Superhydrophobic and Thermal Stable Silica Coating via Sol-Gel Process. *Coatings* **2019**, *9*, 627. [CrossRef]
8. Pantoja, M.; Velasco, F.; Abenojar, J.; Martinez, M.A. Development of superhydrophobic coatings on AISI 304 austenitic stainless steel with different surface pretreatments. *Thin Solid Films* **2019**, *671*, 22–30. [CrossRef]
9. Hu, Y.W.; He, H.R.; Ma, Y.M. Preparation of Superhydrophobic SiO_2 Coating on Stainless Steel Substrate. *Key Eng. Mater.* **2012**, *512*, 1028–1031. [CrossRef]
10. Kwon, M.H.; Shin, H.S.; Chu, C.N. Fabrication of a super-hydrophobic surface on metal using laser ablation and electrodeposition. *Appl. Surf. Sci.* **2014**, *288*, 222–228. [CrossRef]
11. Sahoo, R.K.; Das, A.; Singh, S.K.; Mishra, B.K. Synthesis of surface modified SiC superhydrophobic coating on stainless steel surface by thermal plasma evaporation method. *Surf. Coat. Technol.* **2016**, *307*, 476–483. [CrossRef]
12. Dyrda, K.M.; Grinschek, F.; Rabsch, G.; Haas-Santo, K.; Dittmeyer, R. Development of a microsieve based micro contactor for gas/liquid phase separation. *Sep. Purif. Technol.* **2019**, *220*, 238–249. [CrossRef]
13. Bankovic, P.; Demarquette, N.R.; da Silva, M.L.P. Obtention of selective membranes for water and hydrophobic liquids by plasma enhanced chemical vapor deposition on porous substrates. *Mater. Sci. Eng. B* **2004**, *112*, 165–170. [CrossRef]
14. Robertson, J. Diamond-like amorphous carbon. *Mater. Sci. Eng. R Rep.* **2002**, *37*, 129–281. [CrossRef]
15. Bewilogua, K.; Bialuch, I.; Ruske, H.; Weigel, K. Preparation of a-C:H/a-C:H:Si:O and a-C:H/a-C:H:Si multilayer coatings by PACVD. *Surf. Coat. Technol.* **2011**, *206*, 623–629. [CrossRef]
16. Turri, R.G.; Santos, R.M.; Rangel, E.C.; da Cruz, N.C.; Bortoleto, J.R.R.; Dias da Silva, J.H.; Antonio, C.A.; Durrant, S.F. Optical, mechanical and surface properties of amorphous carbonaceous thin films obtained by plasma enhanced chemical vapor deposition and plasma immersion ion implantation and deposition. *Appl. Surf. Sci.* **2013**, *280*, 474–481. [CrossRef]
17. Santos, R.M.; Turri, R.E.C.; da Cruz, N.C.; Schreiner, W.; Davanzo, C.U.; Durrant, S.F. Diverse Amorphous Carbonaceous Thin Films Obtained by Plasma Enhanced Chemical Vapor Deposition and Plasma Immersion Ion Implantation and Deposition. *Phys. Procedia* **2012**, *32*, 48–57. [CrossRef]
18. Guermat, N.; Bellel, A.; Sahli, S.; Segui, Y.; Raynaud, P. Thin plasma-polymerized layers of hexamethyldisiloxane for humidity sensor development. *Thin Solid Films* **2009**, *517*, 4455–4460. [CrossRef]
19. Smolders, K.; Franken, A.C.M. Terminology for Membrane Distillation. *Desalination* **1989**, *72*, 249–262. [CrossRef]
20. Grischke, M.; Hieke, A.; Morgenweck, F.; Dimigen, H. Variation of the wettability of DLC-coatings by network modification using silicon and oxygen. *Diam. Relat. Mater.* **1998**, *7*, 454–458. [CrossRef]
21. Hubadillah, S.K.; Tai, Z.S.; Othman, M.H.D.; Harun, Z.; Jamalludin, M.R.; Rahman, M.A.; Jaafar, J.; Ismail, A.F. Hydrophobic ceramic membrane for membrane distillation: A mini review on preparation, characterization, and applications. *Sep. Purif. Technol.* **2019**, *217*, 71–84. [CrossRef]
22. Zhang, F.; Chen, S.; Dong, L.; Lei, Y.; Liu, T.; Yin, Y. Preparation of superhydrophobic films on titanium as effective corrosion barriers. *Appl. Surf. Sci.* **2011**, *257*, 2587–2591. [CrossRef]
23. Kulinich, S.A.; Farzaneh, M. Hydrophobic properties of surfaces coated with fluoroalkylsiloxane and alkylsiloxane monolayers. *Surf. Sci.* **2004**, *573*, 379–390. [CrossRef]
24. Lawson, K.W.; Lloyd, D.R. Membrane distillation. *J. Membr. Sci.* **1997**, *124*, 1–25. [CrossRef]
25. Kujawski, W.; Krajewska, S.; Kujawski, M.; Gazagnes, L.; Larbot, A.; Persin, M. Pervaporation properties of fluoroalkylsilane (FAS) grafted ceramic membranes. *Desalination* **2007**, *205*, 75–86. [CrossRef]
26. DIN Deutsches Institut für Normung. Beschichtungsstoffe—Benetzbarkeit—Teil 2: Bestimmung der freien Oberflächenenergie fester Oberflächen durch Messung des Kontaktwinkels. *DIN* **2011**, *2*, 1–18.
27. Shi, P.; Shi, H.; Liu, C.; Jiang, M. Effect of pickling process on removal of oxide layer on the surface of ferritic stainless steel. *Can. Metall. Q.* **2018**, *57*, 168–175. [CrossRef]
28. Decker, E.L.; Garoff, S. Contact Line Structure and Dynamics on Surfaces with Contact Angle Hysteresis. *Langmuir* **1997**, *13*, 6321–6332. [CrossRef]
29. Esih, I.; Alar, V.; Juraga, I. Influence of thermal oxides on pitting corrosion of stainless steel in chloride solutions. *Corros. Eng. Sci. Technol.* **2005**, *40*, 110–120. [CrossRef]
30. Higginson, R.L.; Jackson, C.P.; Murrell, E.L.; Exworthy, P.A.Z.; Mortimer, R.J.; Worrall, D.R.; Wilcox, G.D. Effect of thermally grown oxides on colour development of stainless steel. *Mater. High Temp.* **2015**, *32*, 113–117. [CrossRef]

31. Li, L.; Breedveld, V.; Hess, D.W. Creation of Superhydrophobic Stainless Steel Surfaces by Acid Treatments and Hydrophobic Film Deposition. *ACS Appl. Mater. Interfaces* **2012**, *4*, 4549–4556. [CrossRef] [PubMed]
32. Song, J.-W.; Ma, M.-C.; Fan, L.-W. Understanding the Temperature Dependence of Contact Angles of Water on a Smooth Hydrophobic Surface under Pressurized Conditions: An Experimental Study. *Langmuir* **2020**, *36*, 9586–9595. [CrossRef] [PubMed]
33. García-Payo, M.C.; Izquierdo-Gil, M.A.; Fernández-Pineda, C. Wetting Study of Hydrophobic Membranes via Liquid Entry Pressure Measurements with Aqueous Alcohol Solutions. *J. Colloid Interface Sci.* **2000**, *230*, 420–431. [CrossRef] [PubMed]
34. International Organization for Standarization. *ISO 25178-2. Geometrical Product Specifications (GPS)—Surface Texture: Areal—Part 2: Terms, Definitions and Surfacetexture Parameters*; International Organization for Standarization: Geneva, Switzerland, 2012; Volume 2, pp. 1–47.